

Development of Ultralight Hybrid Pneumatic Artificial Muscle for Large Contraction and High Payload

Seonggun Joe, *Student member, IEEE*, Hongbo Wang, *Member, IEEE*,
Massimo Totaro, *Member, IEEE*, Lucia Beccai, *Member, IEEE*

Abstract—This paper presents a novel pneumatic artificial muscle (PAM) that is able to generate a high payload and buckling pressure. The proposed actuator exploits open-cell foam, and 0.8 mm thick rigid rings to reinforce structure stiffness, and to implement stable contraction under depressurization. All components are embedded in a sealing elastomeric skin. The actuator can support 6.8 N of external load, which is 34.5 times greater than its own weight (20g). When depressurized, the actuator deforms stably, without buckling. The results of the preliminary experimental analysis show that it is able to contract up to 51.8% upon -80 kPa, with a 5.6% hysteresis for pressure vs. contraction ratio. Moreover, a quasi-static model is proposed to estimate the actuator blocking force, of which the measured maximum value is 32.7 N at -80 kPa vacuum. The presented actuator shows repeatable and reliable performance, providing a promising soft material solution for pneumatic driven movement.

Keywords—pneumatic artificial muscles (PAMs), vacuum pressure, ultralight, open-cell foam, bellow, soft actuator

I. INTRODUCTION

In the last decade, soft robotics has shown promising developments to achieve new capabilities, including safe interaction with humans. [1-4]. The implementation of soft movements is paramount to perform new tasks in the environment, and many soft actuators have been investigated with different mechanisms (*i.e.*, Bowden cables [5], piezoelectric actuators [6], Dielectric Elastomer Actuators (DEA) [7], shape memory alloys or polymers [8, 9], ionic polymers [10], and pneumatic actuators [11]). Among them, pneumatic actuation is a versatile, feasible and cost-effective technology for compliant motion, even though it requires bulky air compressors [12, 13]. Pneumatic Artificial Muscles (PAMs) are robust, have high power to mass ratio and high energy efficiency, with a high pulling force. Furthermore, the fabrication of the molds with complex 3D geometries needed to build the soft actuators became easy and fast by means of additive manufacturing techniques. The latter, indeed, can be used to directly fabricate the actuators themselves by carefully tuning the printing parameters for soft materials [14, 15]. Nevertheless, the main challenges in PAMs development are

to achieve large pulling force, deformation, and fast response [16, 17].

The large actuating force, with large contraction or elongation ratio, generally depends on the mechanical behavior of the constituent materials. McKibben actuators with linear contractions were developed not only by reducing the actuator mass, but also by increasing the input power. An example is given by an actuator consisting of a cylindrical flexible rubber or silicone bladder, sheathed with an inextensible fiber network [18, 19]. The inextensible threads in the sheath were bonded on the surface of the elastomeric bladder. In this case, the actuators' performance depends on both the materials properties of the elastomers and the arrangement of the inextensible fibers. Accordingly, by arranging the fibers at an optimal angle and integrating typical elastomers, McKibben actuators can generate large pulling forces (from about one to few hundred N), with large contraction and/or elongation ratios (< 30%) [20- 22].

Combinations of different materials can also be adopted in order to develop origami-inspired and reconfigurable actuators. Various technologies have been used to obtain excellent performance, and to ease the fabrication complexity. For example, Lee *et. al.*, presented an origami-based vacuum pneumatic actuator (OV-PAM) using a Polyvinyl chloride (PVC) film, which generated an extremely large force of 400 N with 90% of contraction ratio [23]. Similarly, Li *et. al.*, developed a longitudinal muscle using a Thermoplastic polyurethane (TPU) coated with nylon fabric [24]. Although the Young's modulus of the employed materials is generally greater than the elastomers, re-configurability was enabled by making foldable lines on the rigid, but thin material layers [25, 26]. However, this solution was too compliant and unreliable for repeated actuation cycles because of stress concentration along the folds and vertices. To release and distribute these stresses, specific hole patterning was employed (this also being useful for structure reinforcement) [25]. However, such patterning can cause the structure to be easily fractured by an externally applied force, and at the same time it makes PAMs implementation challenging.

In the meanwhile, novel flexible structures using elastomers, such as silicone rubber or flexible resin were proposed for artificial muscles [14, 27-30]. Among them, the bellow is one of the most promising structures, since it can generate a large contraction ratio with a light weight, and it has been widely exploited in soft robotics [14, 28, 29]. Charbel Tawk *et. al.*, presented a linear soft vacuum actuator (LSOVA)

*Hongbo Wang would like to thank the financial support of his Marie Skłodowska-Curie Individual Fellowship ("3D-SITS") from the European Union's Horizon 2020 research and innovation programme (No. 799773).

Seonggun Joe is with the Center for Micro-BioRobotics of the Istituto Italiano di Tecnologia (IIT), the BioRobotics Institute of the Scuola Superiore Sant'Anna (SSSA), Pisa, Italy (e-mail: Seonggun.Joe@iit.it).

Hongbo Wang, Massimo Totaro, and Lucia Beccai are with the Center for Micro-BioRobotics of the Istituto Italiano di Tecnologia (IIT), Italy. Corresponding address: Viale Rinaldo Piaggio 34, 56025 Pontedera, PI, Italy; Phone: +39 050 883021. (e-mail: Hongbo.Wang@iit.it, Massimo.Totaro@iit.it, Lucia.Beccai@iit.it)

that was fabricated by 3D printing [14]. One of the versions (5C-LSOVA) was able to contract up to 51.5 % with 27.66 N blocking force, but a large hysteresis occurred because of the buckling of the thin walls. The thin wall was also the reason why the structure could not support a high external force/weight. On the other hand, a Hyper-Elastic Bellow (HEB) actuator was developed by Digumarti *et. al.*, who used both a positive and negative pressure to implement large deformations [29]. They demonstrated that the HEB can achieve a total length change of 450%, with 80% deformation in a radial direction. In summary, such bellow structures are much softer than those previously mentioned. However, as expected, generally the consequences are not only a high hysteresis, but also non-linear deformations. In particular, usually, the resulting actuator is too delicate to support its own weight by the principle of the square-cube law. Namely, if the structure's volume is increased (*i.e.*, in order to maintain its own weight), the flexibility of the structure decreases. Furthermore, this causes undesired deformations (*i.e.*, buckling), even if small external forces are imposed. To reinforce the structure stability and maintain the same elasticity, in previous studies composite materials have been used [24, 31]. However, enhancing stiffness can dramatically affect the mechanical behavior of actuator, especially because this implies an increase of the overall weight, with a consequent decrease in energy efficiency.

In this work, we address these issues and investigate the design factors needed to achieve a reinforced structure but keeping weight ultralight. We design, build and test a novel pneumatic artificial muscle based on open-cell foam with improved axial stiffness, which is capable of generating a large blocking force with a high contraction ratio.

II. DESIGN AND FABRICATION

Foams have promising characteristics (*e.g.*, extremely large deformation, high elasticity, ultralight, etc.) for developing actuation in soft robotics [21]. Foams are typically classified as closed or open cell, according to the configuration of the air cells. In case of closed-cell foams, the air cells are not tangled, like instead happens for the open-cell type (as shown in Fig. 1(b)). In the latter case, upon depressurization, the air cells are compressed, and ultimately, the deformation of the structure occurs. Therefore, the mechanical behavior of the open-cell foam must be evaluated, in order to properly integrate it in the actuator.

A. Mechanical behavior of the open-cell foam

The experimental setup shown in Fig. 1(a) was used to investigate the mechanical behavior of open-cell foam (commercial Polyurethane (PU) foam, 24"x24"x0.5"). It integrates a single-axis load cell (FSH00103, FUTEK, CA, USA) to measure the applied force, and a motorized linear stage (M-111.1DG1, Physik Instrumente, Germany). A plastic cylindrical indenter (25 mm diameter, 10 mm thickness) was used to distribute pressure uniformly on the top surface of the foam samples. The foam samples had a diameter of 20 mm, and 25.5 mm in length. A LabView program was developed for both the data acquisition via NI USB 6218 (National Instruments, TX, USA), and the control of the motor stage. The loading/unloading cycle experiments were repeated 10

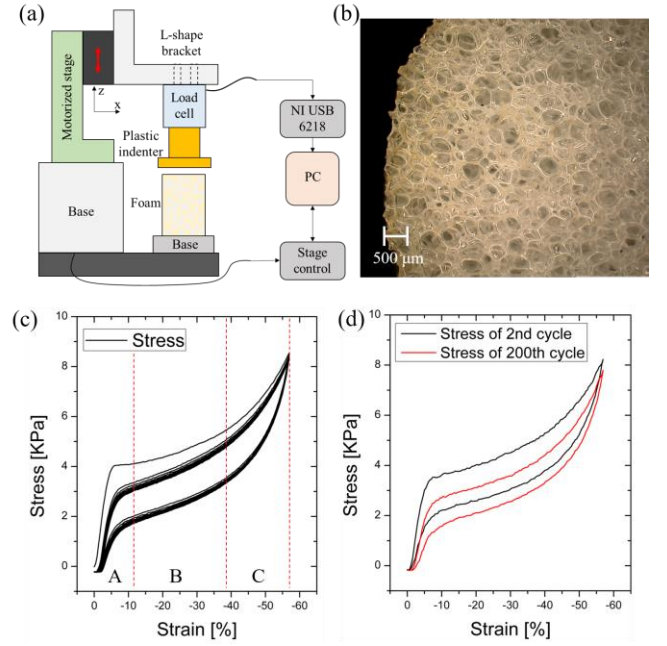


Fig. 1. Compression test of the open-cell foam: (a) experimental setup; (b) image of foam surface taken by digital microscope; (c) strain-stress curve of 10 cycle test (A. Linear elastic region, B. Plateau region, C. Densification region); (d) extrapolated 2nd and 200th cycle test results.

times. As plotted in the graphs of Fig.1(c), the foam behavior was highly viscoelastic (confirming previous results [32, 33]). Three main regimes can be identified: linear elastic region (A); plateau region (B); and, densification region (C). During testing, the foam did not show any sign of failure, even though it was compressed up to 57%. On the other hand, the hysteresis was extremely large. Several studies focused on foam response to different strain, porosity, and temperature [34–36]. In our case, the maximum stress and strain are key parameters for designing the actuator. In addition, we investigated the reliability of the open-cell foam by performing 200 cycling tests for 6 hours, as shown in Fig. 1(d). Results show a hysteresis loss after 200 cycles, while the maximum stress value induced by strain remains almost unchanged.

B. Design and fabrication of the PAM

The PAM was implemented with a bellow architecture and an enveloping skin. The following requirements were considered:

1. The soft skin enveloping the foam-based structure should be made of soft elastomers and able to reach relatively large contraction ratio (up to 50%);
2. The actuator should be ultralight, and able to lift very heavy payload compared to its own weight (at least 10 times);
3. The fabrication should be low-cost and repeatable;
4. The actuator should have a short response time;
5. The deformation of the structure should be predictable by applying both external and internal stimulations (*i.e.* load/weights, vacuum or pneumatic pressure).

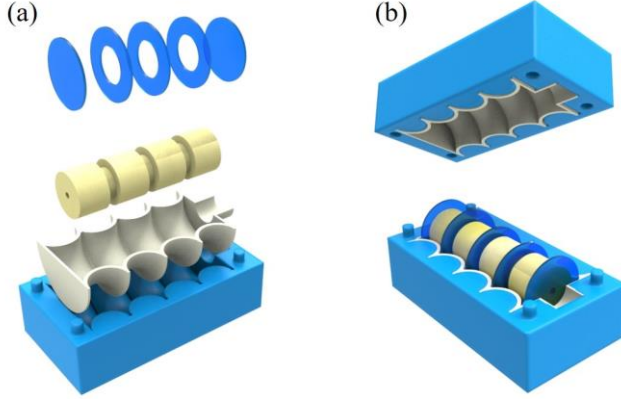


Fig. 2. Fabrication procedure for the artificial muscle: (a) assembly the foam and the rigid mask with the cured elastomeric skin (Dragon Skin 00-30); (d) bonding the skin with the assembled structure.

A conventional bellows structure can be usually actuated by negative or positive pressure. In this study, our objective was to design an actuator working with negative pressure, in order to elicit a fast response, as well as to simplify the control system. However, the axial stiffness of such actuator is generally too low for the PAM to support external loads, including its own weight. Therefore, the mechanical behavior must be investigated.

Two types of PAMs were considered in this analysis: Type 1 was represented by prototypes that did not integrate any rigid ring (but just open-cell foam and elastomeric skin); Type 2 was represented by hybrid prototypes, as shown in Fig.3(a), which integrated both soft and rigid rings.

The main steps of the fabrication process are shown in Fig.2. Symmetrical wax molds were fabricated by 3D printer machine (ProJet MJP 3600, 3D printer, Inc.), and used to fabricate the skin with a thickness of 1 mm with Dragon Skin 30 (Shore 30 A, Smooth-On Inc., Easton, PA, USA). The open-cell foam cylinders (n. 4 having 20 mm diameter, 12.4 mm length; 3 having 11 mm diameter, 6.2 mm length), and 5 rigid rings (28.5 mm diameter, 0.8 mm thick) were patterned by a 2D laser cutter (Versa LASER VLS 3.5). As shown in Fig.2(a), the inner structure was built by bonding all the components by Sil-Poxy (Smooth-On Inc., SIL-Poxy® adhesive). Because the foam absorbs silicone, the skin parts were bonded to the inner structure by brushing the same silicone material of the skin (Dragon Skin 30). After curing of the silicone, both sides were brushed again to bond the two halves of the skin together, as shown in Fig.2(b).

III. STRUCTURAL ANALYSIS

A. Buckling analysis

The methodology consisted in deriving experimentally the axial stiffness for each type of PAM. Typically, the buckling and/or squirm deformation of bellows occurs for an overwhelming compression load. This failure represents the column squirm failure due to insufficient stiffness. Such an undesired deformation causes not only inaccurate control of the structure, but also non-linear behavior of the actuator.

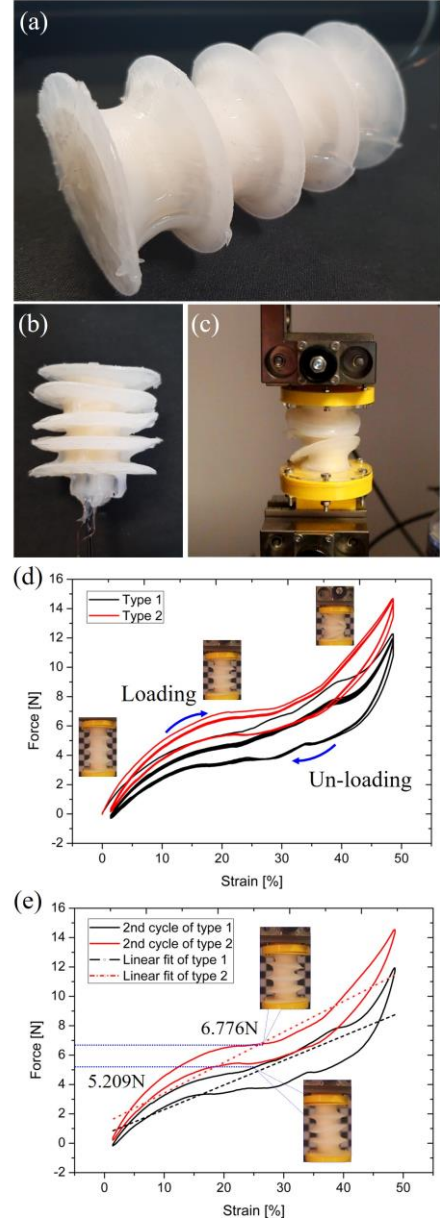


Fig. 3. Experimental results of PAM Type 1 (without rigid rings) and PAM Type 2 (with rigid rings): (a) image showing the fabricated PAM Type 2; (b) PAM Type 2 with vacuum applied; (c) image showing the compression testing at 45% of compression rate; (d) cyclic compression test results; (e) axial stiffness linearly interpolated by LSM (dashed curves) for the 2nd loading/unloading cycle.

Therefore, the critical load to cause buckling had to be evaluated to ensure reliable and stable operation of the proposed actuator.

From a theoretical point of view, the bending stiffness of the bellows C_{bg} is proportional to the axial stiffness [37-39], which can be derived as Eq. (1).

$$C_{bg} = EI = \frac{D_m^2 \cdot h}{8} f_{iu} \quad (1)$$

where E and I are the Young's modulus of material and the moment inertial of structure, respectively; f_{iu} refers to the axial stiffness, and D_m and h are the mean diameter and pitch,

respectively. Then, the buckling pressure (P_c) can be described by:

$$P_c = \frac{\pi \cdot C_{bg}}{D_m^2 \cdot h^2} = \frac{\pi}{8h} f_{iu} \quad (2)$$

From an experimental point of view, f_{iu} can be derived from the average slope of loading-unloading curves. These were obtained for each PAM type by cyclic compression tests, and performed by means of a Zwick/Roell Z005 materials testing machine (Ulm, Germany). As indicated in Fig.3(d), PAM Type 2 has relatively small hysteresis, and much higher axial stiffness.

In order to derive the axial stiffness f_{iu} from experimental cyclic compression data, a linear numerical fitting (Least Square Method) was performed, as shown in Fig.3(e) (plotted in dashed lines). It was assumed that the relation between the strain and the average slope provides the axial stiffness of the viscoelastic structure. Then, these values were used in Eq. (1) and (2) to derive the bending stiffness (C_{bg}) and the buckling pressure (P_c), respectively. In addition, P_c can also be derived experimentally, by observing when the structure starts to buckle during compression tests. Videos were recorded to extract the buckling pressure at the moment when the structure just began to squirm (see the supplementary video). The two theoretical buckling pressures ($P_{c,theo}$) were compared with their experimental correspondent value ($P_{c,exp}$) by means of the above method. The error rates were around 0.57% and 1.86%, for PAMs Type 1 and Type 2, respectively. Furthermore, when the prototypes were fully contracted by depressurization using a syringe, Type 2 showed a uniform deformation, without any buckling, compared to Type 1, as illustrated in Fig. 3(b).

Hence, this indicated that Type 2 had an improved axial stiffness compared to Type 1. All key parameters to compare the performance of the hybrid versus the entirely soft PAM are summarized in Table 1.

In summary, results show that the proposed Ultralight Hybrid Pneumatic Artificial Muscles (UH-PAMs) Type 2 can support 6.8 N axially, which is 34.5 times greater than its own

weight (20g). In addition, 4.9 kPa buckling pressure of Type 2 is higher than that of Type 1 by 30%.

B. Quasi-static model to approximate blocking force

The mechanical behavior of the proposed actuator can be approximated using a quasi-static model [14, 23]. The main assumption, as illustrated in Fig.4 is that the distributed pressure acting on the inner wall of the structure is equal to the weight that the muscle can lift:

$$-F \cdot dh = P \cdot dv \quad (3)$$

where F and dh are the blocking force owing to the applied vacuum pressure, and linear displacement, respectively. Otherwise, P and dv are the gauge pressure and the change in the volume of the actuator, respectively. Here, the friction between the foam and structure, and the density and the viscosity of working fluid are neglected.

To derive the function of compressive force with respect to the displacement, the arc-length of an ellipse (l) is approximated as the initial circular length ($l_0 = \pi r$). The length of the major axis α can be approximated as

$$\alpha \cong \sqrt{\left(\frac{2l_0^2}{\pi^2} - \frac{h^2}{4}\right)} \quad (4)$$

Then, its differential equation, which indicates the ratio of the contraction in radial and longitudinal directions C_R , can be written as

$$C_R = \frac{d\alpha}{dh} = -\frac{1}{4}h \frac{1}{\sqrt{\left(\frac{2l_0^2}{\pi^2} - \frac{h^2}{4}\right)}} = -\frac{h}{4\alpha} \quad (5)$$

Therefore, the volume variation of the single convoluted cell as a function of the displacement can be written by the partial differentiation

$$\frac{dv}{dh} = \frac{\pi D^2}{8} - \frac{2\pi}{3} ah \cdot \frac{d\alpha}{dh} - \frac{\pi}{3} \alpha^2 \quad (6)$$

TABLE I. DESIGN PARAMETERS AND RESULTS OF THE BUCKLING ANALYSIS

Nomenclature	Dimension	Type 1	Type 2
Diameter (D)	[mm]	42	
Mean Diameter (D_m)	[mm]	33.5	
Pitch (h)	[mm]	17	
Radius of curvature (r)	[mm]	8.5	
Number of convolutions [n]	[turns]	4	
Total length (H)	[mm]	72	
Axial stiffness (f_{iu})	[N/mm]	0.1673	0.20779
Bending stiffness (C_{bg})	[N·mm ²]	398.974	495.534
Theoretical buckling pressure ($P_{c,theo}$)	[kPa]	3.865	4.80
Experimental buckling pressure ($P_{c,exp}$)	[kPa]	3.760	4.891
Error rate (e)	[%]	2.788	1.859

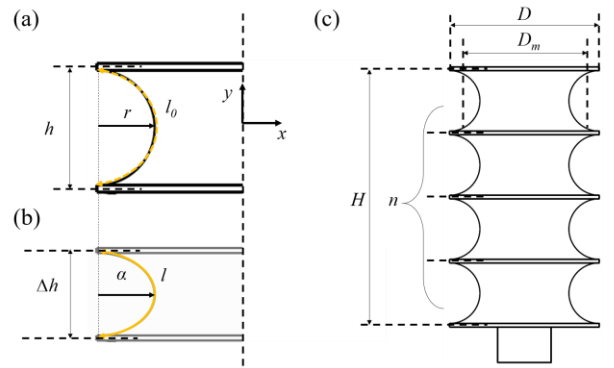


Fig. 4. Parameters of the artificial muscle for quasi-static model: (a) side views of single segment at initial (a) and at compressed (b) state; (c) schematics of fully assembled artificial muscle.

Finally, by substituting Eq. (5) and (6), the blocking force as a function of displacement h can be derived as

$$F(h) = -P \cdot \frac{dv}{dh} = -P \cdot \left[\frac{\pi D^2}{8} + \frac{\pi h^2}{6} - \frac{\pi}{3} \alpha^2 \right] \quad (7)$$

C. Characterization of UH-PAM

The actuator's behavior was characterized experimentally, and compared with the quasi-static numerical model described in the aforementioned section.

An experimental setup was built to measure the contraction ratio and the blocking force. The pressure for the artificial muscle actuation was tuned by a vacuum flow regulator (ITV0090, SMC corporation), with a maximum vacuum of 100 mbar generated by a vacuum pump (Diaphragm Vacuum Pumps and compressor, N022 AN.18, KNF LAB). The data acquisition and analog signal output were implemented by DAQ6218 (National Instruments, TX, USA). The kinematic characteristics of the actuator were obtained by AURORA tracking system (AURORA® EM), which records 6 degrees-of-freedom through a localization probe (Northern Digital Inc.). To investigate the blocking force delivered by the artificial muscle, both rigid terminals of the muscle were clamped, as shown in Fig.6, with the actuator at the unpressurized state. Then, the force was measured using a load cell (Zwick/Roell Xforce Load cell, F max 50 N, 3001493, Ulm, Germany) and increasing the vacuum pressure from 0 kPa to -80 kPa, with steps of -5 kPa.

IV. RESULTS

Static characteristics; The proposed UH-PAM can produce relatively large displacement at small pressure (<20 kPa), similarly to some of the reported PAM [11, 23, 29]. Furthermore, the UH-PAM is capable of a contraction ratio up to 51.8% at -80 kPa, and showed non-linear behavior for the pressure ranging from 0 to -80 kPa, as shown in Fig.5. The pressure curve (function of the contraction ratio) shows a hysteresis of 5.6%, which is much smaller than currently reported soft actuators (*i.e.* over 75%) [14].

Blocking force; Fig.6 shows that the blocking force is linearly proportional to the applied vacuum pressure, with a maximum blocking force of 32.7 N at -80 kPa. Indeed, the agreement between experimental data (black squared marks) and the quasi-static model (red dashed line) is very good, with

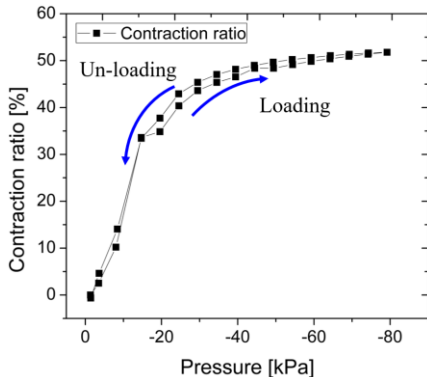


Fig. 5. Contraction ratio as a function of vacuum pressure for loading and un-loading cycle.

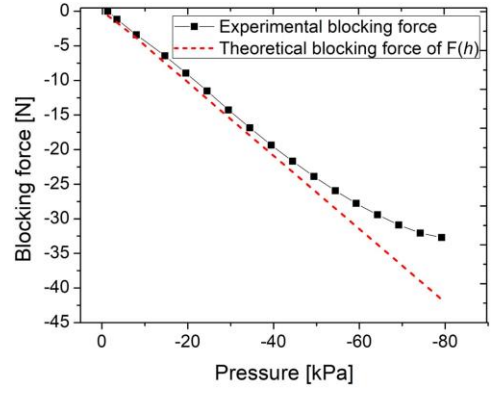


Fig. 6. Experimental (black square marked line) and theoretical (red dashed line) blocking force under vacuum pressure from 0 to -80 kPa.

an error less than 10.4 % up to -65 kPa, and a maximum error of 27.4% at -80 kPa. This indicates that the assumption of constant arc-length of ellipse in the quasi-static model is suitable.

V. CONCLUSION

In this paper, we investigated the mechanical behavior of UH-PAM based on open-cell foams. The foam viscoelastic behavior in compression dominantly affects the mechanical behavior of the actuator. Consequently, the contraction ratio, as a function of the vacuum pressure, has a non-linear behavior. We analyzed the buckling pressure causing lateral squirmed deformation, and concluded that the proposed muscle could support about 6.8 N of external load, which is around 34.5 times of its own weight (20 g). Furthermore, the rigid rings were employed to prevent not only the lateral squirm deformation of the structure, but also to reduce its hysteresis. In particular, the axial stiffness and the bending stiffness of the UH-PAM were increased by 24.2%, compared with PAM without rigid rings. Based on a quasi-static model, we estimated the blocking force of the UH-PAM as a function of the vacuum pressure. The maximum blocking force of the actuator is 32.7 N, which is more than 166 times its own weight.

In summary, the proposed UH-PAM shows promising characteristics that could be exploited in several applications. One of the potentialities of this approach is the possibility, in a near future, to integrate foam-based deformation sensing [40], in order to enable closed-loop control.

The results of this work show that the UH-PAM exhibits large contraction upon application of vacuum pressure, while at the same time, it can support external force/weight with a high buckling pressure. Starting from these encouraging results, more comprehensive studies on the bellow skin and on the composite structure will be conducted. They will focus on the mechanical behavior of the UH-PAM, exploiting different elastomeric materials, foams and rigid rings, both experimentally and through numerical simulations. Based on the above evaluation and optimization, a complete investigation under different conditions will be performed, and the UH-PAMs will be integrated in soft robots and manipulators, to demonstrate their feasibility for such applications.

REFERENCES

- [1] T. Ranzani, G. Gerboni, M. Cianchetti, and A. Menciassi, "A bioinspired soft manipulator for minimally invasive surgery," *Bioinspiration & Biomimetics*, vol. 10, no. 3, p. 035008, 2015.
- [2] F. Renda, M. Cianchetti, M. Giorelli, A. Arienti and C. Laschi, "A 3D steady-state model of a tendon-driven continuum soft manipulator inspired by the octopus arm." *Bioinspiration & biomimetics* vol 7, no. 2, p. 025006, 2012.
- [3] C. Laschi, M. Cianchetti, B. Mazzolai, L. Margheri, M. Follador, and P. Dario, "Soft Robot Arm Inspired by the Octopus," *Advanced Robotics*, vol. 26, no. 7, pp. 709–727, 2012.
- [4] C. Laschi, B. Mazzolai, and M. Cianchetti, "Soft robotics: Technologies and systems pushing the boundaries of robot abilities," *Science Robotics*, vol. 1, no. 1, p. eaah3690, 2016.
- [5] M. Xiloyannis, L. Cappello, Dinh Binh Khanh, Shih-Cheng Yen, and L. Masia, "Modelling and design of a synergy-based actuator for a tendon-driven soft robotic glove," in 2016 6th IEEE International Conference on Biomedical Robotics and Biomechatronics (BioRob), 2016.
- [6] A. Zolfagharian, A. Z. Kouzani, S. Y. Khoo, A. A. A. Moghadam, I. Gibson, and A. Kaynak, "Evolution of 3D printed soft actuators," *Sensors and Actuators A: Physical*, vol. 250, pp. 258–272, 2016.
- [7] C. Christianson, N. N. Goldberg, D. D. Deheyne, S. Cai, and M. T. Tolley, "Translucent soft robots driven by frameless fluid electrode dielectric elastomer actuators," *Science Robotics*, vol. 3, no. 17, p. eaat1893, 2018.
- [8] M. Cianchetti, A. Licofonte, M. Follador, F. Rogai, and C. Laschi, "Bioinspired Soft Actuation System Using Shape Memory Alloys," *Actuators*, vol. 3, no. 3, pp. 226–244, 2014.
- [9] K. Takashima, J. Rossiter, and T. Mukai, "McKibben artificial muscle using shape-memory polymer," *Sensors and Actuators A: Physical*, vol. 164, no. 1–2, pp. 116–124, 2010.
- [10] K. Takagi, M. Yamamura, Z. Luo, M. Onishi, S. Hirano, K. Asaka, Y. Hayakawa, "Development of a Rajiform Swimming Robot using Ionic Polymer Artificial Muscles," in 2006 IEEE/RSJ International Conference on Intelligent Robots and Systems, 2006.
- [11] K. C. Wickramatunge and T. Leephakpreeda, "Study on mechanical behaviors of pneumatic artificial muscle," *International Journal of Engineering Science*, vol. 48, no. 2, pp. 188–198, 2010.
- [12] D. Bou Saba, P. Massioni, E. Bideaux, and X. Brun, "Flatness-Based Control of a Two Degrees-of-Freedom Platform With Pneumatic Artificial Muscles," *Journal of Dynamic Systems, Measurement, and Control*, vol. 141, no. 2, 2018.
- [13] F. Daerden, D. Lefeber, "Pneumatic artificial muscles: actuators for robotics and automation," *European journal of mechanical and environmental engineering* vol. 47, no. 1 pp. 11-21, 2002.
- [14] C. Tawh, G. M. Spinks, M. in het Panhuis, and G. Alici, "3D Printable Linear Soft Vacuum Actuators: Their Modeling, Performance Quantification and Application in Soft Robotic Systems," *IEEE/ASME Transactions on Mechatronics*, vol. 24, no. 5, pp. 2118–2129, 2019.
- [15] L. Zhou, Q. Gao, J. Fu, Q. Chen, J. Zhu, Y. Sun, and Y. He, "Multimaterial 3D Printing of Highly Stretchable Silicone Elastomers," *ACS Applied Materials & Interfaces*, vol. 11, no. 26, pp. 23573–23583, 2019.
- [16] H. Wang, M. Totaro, and L. Beccai, "Toward Perceptive Soft Robots: Progress and Challenges," *Advanced Science*, vol. 5, 1800541, 2018.
- [17] S. M. Mirvakili and I. W. Hunter, "Artificial Muscles: Mechanisms, Applications, and Challenges," *Advanced Materials*, vol. 30, no. 6, p. 1704407, 2017.
- [18] N. C. Goulbourne, S. Son, and J. W. Fox, "Self-sensing McKibben actuators using dielectric elastomer sensors," in *Electroactive Polymer Actuators and Devices (EAPAD) 2007*, 2007.
- [19] Nakamura, N. Saga, and K. Yaegashi, "Development of a pneumatic artificial muscle based on biomechanical characteristics," in *IEEE International Conference on Industrial Technology*, 2003.
- [20] B. Tondu, "Modelling of the McKibben artificial muscle: A review," *Journal of Intelligent Material Systems and Structures*, vol. 23, no. 3, pp. 225–253, 2012.
- [21] M. A. Robertson and J. Paik, "New soft robots really suck: Vacuum-powered systems empower diverse capabilities," *Science Robotics*, vol. 2, no. 9, p. eaan6357, 2017.
- [22] P. Boyraz, G. Runge, and A. Raatz, "An Overview of Novel Actuators for Soft Robotics," *Actuators*, vol. 7, no. 3, p. 48, 2018.
- [23] J.-G. Lee and H. Rodrigue, "Origami-Based Vacuum Pneumatic Artificial Muscles with Large Contraction Ratios," *Soft Robotics*, vol. 6, no. 1, pp. 109–117, 2019.
- [24] S. Li, D. M. Vogt, D. Rus, and R. J. Wood, "Fluid-driven origami-inspired artificial muscles," *Proceedings of the National Academy of Sciences*, vol. 114, no. 50, pp. 13132–13137, 2017.
- [25] D.-Y. Lee, S.-R. Kim, J.-S. Kim, J.-J. Park, and K.-J. Cho, "Origami Wheel Transformer: A Variable-Diameter Wheel Drive Robot Using an Origami Structure," *Soft Robotics*, vol. 4, no. 2, pp. 163–180, 2017.
- [26] J. Morgan, S. P. Magleby, R. J. Lang, and L. L. Howell, "A Preliminary Process for Origami-Adapted Design," in *Volume 5B: 39th Mechanisms and Robotics Conference*, 2015.
- [27] H. Tian, Z. Wang, Y. Chen, J. Shao, T. Gao, and S. Cai, "Polydopamine-Coated Main-Chain Liquid Crystal Elastomer as Optically Driven Artificial Muscle," *ACS Applied Materials & Interfaces*, vol. 10, no. 9, pp. 8307–8316, 2018.
- [28] R. Nakayama, R. Suzuki, S. Nakamaru, R. Niiyama, Y. Kawahara, and Y. Kakehi, "MorphIO," in *Proceedings of the 2019 on Designing Interactive Systems Conference - DIS '19*, 2019.
- [29] K. M. Digumarti, A. T. Conn, and J. Rossiter, "Euglenoid-Inspired Giant Shape Change for Highly Deformable Soft Robots," *IEEE Robotics and Automation Letters*, vol. 2, no. 4, pp. 2302–2307, 2017.
- [30] E. H. Skorina et al., "Reverse pneumatic artificial muscles (rPAMs): Modeling, integration, and control," *PLOS ONE*, vol. 13, no. 10, p. e0204637, 2018.
- [31] L. Paez, G. Agarwal, and J. Paik, "Design and Analysis of a Soft Pneumatic Actuator with Origami Shell Reinforcement," *Soft Robotics*, vol. 3, no. 3, pp. 109–119, 2016.
- [32] B. J. Ramirez, U. Misra, and V. Gupta, "Viscoelastic foam-filled lattice for high energy absorption," *Mechanics of Materials*, vol. 127, pp. 39–47, 2018.
- [33] M. Alzoubi, S. Khateeb, and S. Al-Hallaj, "Modeling of compression curves of phase change graphite composites using Maxwell and Kelvin models," *Journal of Composite Materials*, vol. 50, no. 8, pp. 1123–1135, 2015.
- [34] A. Pellegrino, V. L. Tagarielli, R. Gerlach, and N. Petrinic, "The mechanical response of a syntactic polyurethane foam at low and high rates of strain," *International Journal of Impact Engineering*, vol. 75, pp. 214–221, 2015.
- [35] G. Subhash, Q. Liu, and X.-L. Gao, "Quasistatic and high strain rate uniaxial compressive response of polymeric structural foams," *International Journal of Impact Engineering*, vol. 32, no. 7, pp. 1113–1126, 2006.
- [36] C. Salisbury, D. Cronin, and F.-S. Lien, "Deformation Mechanics of a Non-Linear Hyper-Viscoelastic Porous Material, Part II: Porous Material Micro-Scale Model," *Journal of Dynamic Behavior of Materials*, vol. 1, no. 3, pp. 249–258, 2015.
- [37] D. E. Newland, "Buckling of Double Bellows Expansion Joints under Internal Pressure," *Journal of Mechanical Engineering Science*, vol. 6, no. 3, pp. 270–277, 1964.
- [38] C. Becht, IV, "An Evaluation of EJMA Stress Calculations for Unreinforced Bellows," *Journal of Pressure Vessel Technology*, vol. 124, no. 1, pp. 124–129, 2001.
- [39] N. W. Snedden, "Analysis and design guidance for the lateral stiffness of bellows expansion joints," *Thin-Walled Structures*, vol. 3, no. 2, pp. 145–162, 1985.
- [40] H. Wang, I. Bernardeschi, and L. Beccai, "Developing Reliable Foam Sensors with Novel Electrodes," in *2019 IEEE SENSORS*, pp. 1–4, 2019.